Progress in Biophysics and Molecular Biology 129 (2017) 40–52

Contents lists available at ScienceDirect

Progress in Biophysics and Molecular Biology

journal homepage: www.elsevier.com/locate/pbiomolbio

Electrophysiological properties of computational human ventricular cell action potential models under acute ischemic conditions

Sara Dutta [a, *], Ana Mincholé [a], T. Alexander Quinn [b], Blanca Rodriguez [a]

[a] Department of Computer Science, University of Oxford, Oxford, UK
[b] Department of Physiology and Biophysics, Dalhousie University, Halifax, Canada

ARTICLE INFO

Article history:
Received 1 August 2016
Received in revised form
30 December 2016
Accepted 15 February 2017
Available online 20 February 2017

Keywords:
Arrhythmias
Action potential duration
Conduction velocity
Myocardial ischemia
Human ventricular cell models
Refractory period

ABSTRACT

Acute myocardial ischemia is one of the main causes of sudden cardiac death. The mechanisms have been investigated primarily in experimental and computational studies using different animal species, but human studies remain scarce. In this study, we assess the ability of four human ventricular action potential models (ten Tusscher and Panfilov, 2006; Grandi et al., 2010; Carro et al., 2011; O'Hara et al., 2011) to simulate key electrophysiological consequences of acute myocardial ischemia in single cell and tissue simulations. We specifically focus on evaluating the effect of extracellular potassium concentration and activation of the ATP-sensitive inward-rectifying potassium current on action potential duration, post-repolarization refractoriness, and conduction velocity, as the most critical factors in determining reentry vulnerability during ischemia. Our results show that the Grandi and O'Hara models required modifications to reproduce expected ischemic changes, specifically modifying the intracellular potassium concentration in the Grandi model and the sodium current in the O'Hara model. With these modifications, the four human ventricular cell AP models analyzed in this study reproduce the electrophysiological alterations in repolarization, refractoriness, and conduction velocity caused by acute myocardial ischemia. However, quantitative differences are observed between the models and overall, the ten Tusscher and modified O'Hara models show closest agreement to experimental data.

Contents

1. Introduction 41
2. Methods 41
   2.1. Human ventricular cell models 41
   2.2. Ischemic electrophysiological changes 41
   2.3. Modifications to the ORd and GPB models 42
   2.4. Stimulation protocols and electrophysiological measurements 42
   2.5. Numerical methods 42
3. Results 42
   3.1. AP and ionic currents under control and ischemic conditions 42
   3.2. APD and resting membrane potential under varying ischemic conditions 45
   3.3. PRR under varying ischemic conditions 45
   3.4. CV, upstroke velocity and peak voltage under varying ischemic conditions 46
   3.5. APD and CV restitution curves under control and ischemic conditions 47
   3.6. Comparison to experimental data 47
4. Discussion 49
   4.1. All models reproduce ischemia-induced changes 49
   4.2. Comparison between experimental and simulation data 50

* Corresponding author. Department of Computer Science, University of Oxford, Parks Road, OX1 3QD, Oxford, United Kingdom.
E-mail address: sara.dutta@cs.ox.ac.uk (S. Dutta).

http://dx.doi.org/10.1016/j.pbiomolbio.2017.02.007

5. Conclusions 50
Acknowledgements 50
Supplementary data 50
Disclosures 50
Funding sources 50
References 50

1. Introduction

One of the major causes of sudden cardiac death is acute myocardial ischemia, resulting from an imbalance in the supply and demand of oxygen and nutrients to the heart. During the first 10–15 min of ischemia, metabolic and electrophysiological changes occur rapidly and vary spatially, resulting in a shortening of action potential duration (APD), a prolongation of effective refractory period (ERP) beyond APD (termed post-repolarization refractoriness, PRR), and a reduction of AP upstroke and conduction velocity (CV) compared to normal tissue (Sutton et al., 2000; Taggart, 2000). The resulting electrophysiological heterogeneities between normal and ischemic tissue provide the substrate for reentrant arrhythmias, as demonstrated in experimental and simulation studies (Dutta et al., 2016; Janse and Wit, 1989; Pogwizd and Corr, 1987; Tice et al., 2007). Previous research has shown that these changes are mainly caused by: hyperkalemia (increased extracellular potassium concentration, $[K^+]_o$) (Pandit et al., 2010; Schaapherder et al., 1990), which results in an increase in cell resting membrane potential and decreased cell excitability; hypoxia (inadequate supply of oxygen) (Van Wagoner and Lamorgese, 1994; Weiss et al., 1992), which results in an opening of ATP-sensitive inward-rectifying potassium current ($I_{K(ATP)}$) channels; and acidosis (reduced intracellular pH) (Sato et al., 1985; Yatani et al., 1984), which decreases the conductance of the sodium (I_{Na}) and L-type calcium (I_{CaL}) currents (Carmeliet, 1999). However, ischemia is a complex and dynamic process, which needs to be further investigated for a better understanding of ischemia-induced arrhythmia mechanisms.

Most research on ischemia has been carried out in animals (Carmeliet, 1999; Coronel et al., 1988; Fiolet et al., 1985; Furukawa et al., 1991; Ma and Wang, 2007; Pandit et al., 2011; Schaapherder et al., 1990; Wilensky et al., 1986), and data from human is scarce (Sutton et al., 2000; Taggart, 2000). Therefore, extrapolation of mechanisms from animal to human is challenging, but can be facilitated by computational modeling using multi-scale human-specific models (Rodriguez et al., 2016). These computational models provide a flexible platform to impose specific changes not possible in experimental studies and dissect mechanisms with high spatio-temporal resolution, to increase our understanding of ischemia-induced arrhythmic mechanisms in human. Most human models, however, have been created and evaluated using data from healthy cells and their applicability for simulations of ischemia is currently unknown. Therefore, it is important to assess their behavior under varied ischemic conditions, as the ischemic changes described above vary through time and space in and around the ischemic area (Coronel et al., 1988; Fiolet et al., 1985; Schaapherder et al., 1990; Wilensky et al., 1986). Furthermore, even species-specific (e.g., human) models are based on experimental data acquired from different species (e.g., rabbit, pig, etc.) (Niederer et al., 2009); a comparison and assessment between the different model outputs and to experimental data is thus necessary, especially under varying conditions such as ischemia, as has been done in previous studies (Cherry and Fenton, 2007; Gemmell et al., 2016; O'Hara and Rudy, 2012; ten Tusscher et al., 2006).

The aim of this study is to investigate the response of the four most recent computational human-specific ventricular action potential (AP) models (the ten Tusscher and Panfilov, 2006; Grandi et al., 2010; Carro et al., 2011; O'Hara et al. 2011 models) to varied ischemic conditions by comparing electrophysiological properties in single cell and tissue simulations in order to assess their utility for studying mechanisms of arrhythmogenesis during the initial phase of acute myocardial ischemia.

2. Methods

2.1. Human ventricular cell models

Four human ventricular models were investigated in this study: the ten Tusscher et al., the Grandi et al., the Carro et al., and the O'Hara et al. models (Carro et al., 2011; Grandi et al., 2010; O'Hara et al., 2011; ten Tusscher and Panfilov, 2006); a detailed description of the models can be found in the original publications. The ten Tusscher et al. (TP06) model is the most widely used and studied human model, it is based on a previous human model from the same group (ten Tusscher et al., 2004). However, the model does not adequately reproduce AP response to frequency changes and block of potassium currents. The Grandi et al. model (GPB), based on a previously developed rabbit cell model (Shannon et al., 2004), overcomes limitations of the TP06 model. However, based on an analysis of GPB APD restitution and rate adaptation shortcomings, Carro et al. (CRLP) modified and reformulated various currents, including I_{CaL} and the inward rectifying potassium current, I_{K1}; although the CRLP calcium dynamics still needs further improvement compared to the TP06 calcium dynamics. Finally, the most recent human cell model is the O'Hara et al., 2011 model (ORd) (O'Hara et al., 2011), based on human data obtained from over 100 undiseased human hearts. Most notably, the model incorporates the effects of Ca^{2+}/calmodulin-dependent protein kinase II (CaMK) on known ionic currents. Nonetheless, the model is limited in simulating hyperkalemia in tissue, as the model does not reproduce propagation of excitation for $[K^+]_o \geq 6$ mM; an issue that we address in this study.

2.2. Ischemic electrophysiological changes

The $I_{K(ATP)}$ current: $I_{K(ATP)} = G_{K(ATP)} f_{K(ATP)} \left(\frac{[K^+]_o}{[K^+]_{o,n}}\right)^{0.24} (V_m - E_K)$, was based on a previous formulations (Ferrero et al., 1996; Michailova et al., 2007; Shaw and Rudy, 1997) and added to the cell models using COR (Garny et al., 2003). The amplitude of the current depends on the ratio of the present $[K^+]_o$, and the control value of $[K^+]_o$ ($[K^+]_{o,n}$). It also depends on the membrane potential of the cell, V_m, and the Nernst potential of potassium, E_K. We used the value estimated by Michailova et al. (2007). for the channel conductance ($G_{K(ATP)} = 0.05$ mS/μF) and used $f_{K(ATP)}$ as a scaling factor to vary peak $I_{K(ATP)}$ conductance in the models.

We simulated the electrophysiological consequences of the

initial phase of acute myocardial ischemia (first 10–15 min), the time period with highest arrhythmic risk following the onset of ischemia (Carmeliet, 1999; Janse and Wit, 1989; Kazbanov et al., 2014; Trénor et al., 2005), as in previous computational (Heidenreich et al., 2012; Tice et al., 2007; Trénor et al., 2005) and experimental (Irisawa and Sato, 1986; Sato et al., 1985; Yatani et al., 1984) studies. Hyperkalemia and hypoxia are the two major ischemic conditions affecting APD and PRR, important determinants of reentry during ischemia, and were simulated through changes in $[K^+]_o$ and $I_{K(ATP)}$. They were varied to cover the range of values observed experimentally from control to ischemic conditions (Carmeliet, 1999; Coronel, 1994; Van Wagoner and Lamorgese, 1994; Weiss and Shine, 1982) and to reproduce gradients that are observed at the border zone between the ischemic central area and healthy tissue (Coronel, 1994; Schaapherder et al., 1990; Wilensky et al., 1986); a highly heterogeneous region that is prone to ectopic beats and plays an important role in arrhythmogenesis (Bernus et al., 2005; Coronel et al., 1991). $[K^+]_o$ was increased from 4 to 9 mM, in steps of 1 mM, and $I_{K(ATP)}$ peak conductance (varied through $f_{K(ATP)}$) was increased from 0 to 0.2, in steps of 0.02 in single cell and 0.04 in tissue. Peak I_{Na} and I_{CaL} conductances were decreased by 25% in all simulations and were not varied, as they play a smaller role in modulating APD and PRR compared to $[K^+]_o$ and $I_{K(ATP)}$ (Tice et al., 2007; Yatani et al., 1984).

2.3. Modifications to the ORd and GPB models

The original versions of the ORd and GPB models display certain limitations when simulating ischemia: the ORd model does not reproduce PRR in single cell, nor propagation of excitation during hyperkalemia in tissue, while the GPB model does not show excitation propagation for $[K^+]_o$ greater than 8 mM. In order to overcome the limitations of these two models for simulations of ischemia, the I_{Na} formulation and the intracellular potassium concentration ($[K^+]_i$) were modified in the ORd and the GPB models, respectively. As suggested by O'Hara in a comment on the ORd model, the I_{Na} formulation was replaced by the TP06 I_{Na} formulation (referred to here as the ORd (TP06 I_{Na}) model). Under normal conditions, as described by Elshrif and Cherry, the ORd (TP06 I_{Na}) model reproduces a more physiologic CV compared to the original ORd model, while leaving the main other action potential features unchanged (Elshrif and Cherry, 2014). In addition, we developed an adaptation of the original ORd model (referred to as ORd (modified I_{Na}) model), which preserves the CaMK effects on I_{Na} included in the original ORd model (Wagner et al., 2006), by only changing the I_{Na} inactivation gates. Specifically, we changed the steady state of the inactivation h gate as in (Passini et al., 2016) and further improved tissue propagation under hyperkalemia by modifying the time constants of the inactivation gates to match the TP06 I_{Na} formulation (see supplemental material). These changes allow the new versions of the ORd model to overcome limitations of the original model, namely to reproduce the observed increase in PRR under ischemic conditions in single cell, as well as to allow activation propagation in tissue with elevated $[K^+]_o$. Finally, the $[K^+]_i$ of the original GPB model was changed from 120 to 138 mM as in the CRLP model, allowing the new GPB model to show propagation of excitation in tissue for $[K^+]_o = 9$ mM (this is not the case with the original GPB model).

2.4. Stimulation protocols and electrophysiological measurements

Single cell simulations were run to steady state for 1000 beats with a 1 ms stimulus of −50 μA/μF applied every 1000 ms, set at two times control diastolic threshold as in (Sutton et al., 2000). Tissue simulations were run in a 5 cm long strand of tissue for 5 beats with a 0.5 ms stimulus of -10^6 μA/cm^3 (equivalent to −714 μA/μF given a surface area to volume ratio of 1400 cm^{-1} and a capacitance of 1 μF/cm^2) applied every 1000 ms to the cell at position x = 0 cm. Both in single cell and tissue simulations the electrophysiological properties were calculated using the last beat. AP amplitude (APA) was calculated as the difference between the peak and resting membrane potential (V_{rest}) during the last beat. APD was calculated as the difference between the time of maximum upstroke velocity and the time when the cell repolarizes to 90% of its APA. ERP was calculated once the cell was at steady state by applying a stimulus at progressively shorter coupling intervals (S2), with 10 ms precision. In single cell, ERP was defined as the minimum S2 coupling interval (greater than the APD) that triggered an AP (defined as having a plateau above −20 mV). In tissue simulations, ERP was defined by the minimum S2 coupling interval that triggered an AP in the cell at position x = 3 cm. The PRR was calculated as the difference between ERP and APD. CV was calculated between the cell at position 1 cm and the cell at position 3 cm as the difference in time of maximum upstroke velocity (dV/dt_{max}) at each position divided by the distance between the two cells. APD and CV restitution curves were calculated in tissue by pacing for 5 beats with a coupling interval of 1000 ms and then delivering a progressively shorter S2 coupling interval (in 100 ms increments) until propagation failure. Convergence of tissue simulations results was assessed by comparing metrics after 5, 10 and 100 beats under ischemic conditions ($[K^+]_o = 9$ mM and $f_{K(ATP)} = 0.2$); all models showed a change of less than 3% in CV, APD90 and V_{rest} when 5 and 100 beats were compared.

2.5. Numerical methods

Single cell simulations were run in MATLAB for all models. Equations were solved using *ode15s* with a maximum time step of 1 ms, and a relative and absolute tolerance of 10^{-7} and 10^{-9} to ensure numerical convergence. Tissue simulations were run using Chaste (Pitt-Francis et al., 2009) with a space discretization of 0.01 cm. The ODE and PDE time steps were set to 0.001 ms and 0.01 ms for all the models, which ensured convergence of results. The forward Euler method was used to solve the set of ODEs and the monodomain model described the electrical activity of the myocardium through a parabolic differential equation, which was solved using the finite element method (Bernabeu et al., 2014, p. 20; Pathmanathan et al., 2010).

3. Results

3.1. AP and ionic currents under control and ischemic conditions

Fig. 1 shows the AP, transient outward potassium current (I_{to}), rapid (I_{Kr}) and slow (I_{Ks}) delayed rectifier potassium current, I_{Na} and I_{CaL} traces for all models under control ($[K^+]_o = 4$ mM and $f_{K(ATP)} = 0$) and ischemic ($[K^+]_o = 9$ mM and $f_{K(ATP)} = 0.2$) conditions. We notice that all models display different AP and current morphologies in both control and ischemic conditions. For example, the GPB and CRLP models have a longer control APD than the other models, due to a lower I_{Kr} current; however, under ischemic conditions all models show similar APDs. Furthermore, the TP06 AP has a more pronounced notch and plateau phase compared to the other models, due to its higher I_{CaL} and I_{to} currents, both in control and ischemia. There are no clear differences in AP morphology between the original ORd model and the ORd (TP06 I_{Na}) and ORd (modified I_{Na}) models, apart from the AP peak amplitude due to the changes in I_{Na}. Finally, as expected under ischemic conditions, in all models, the APD decreases and V_{rest} increases.

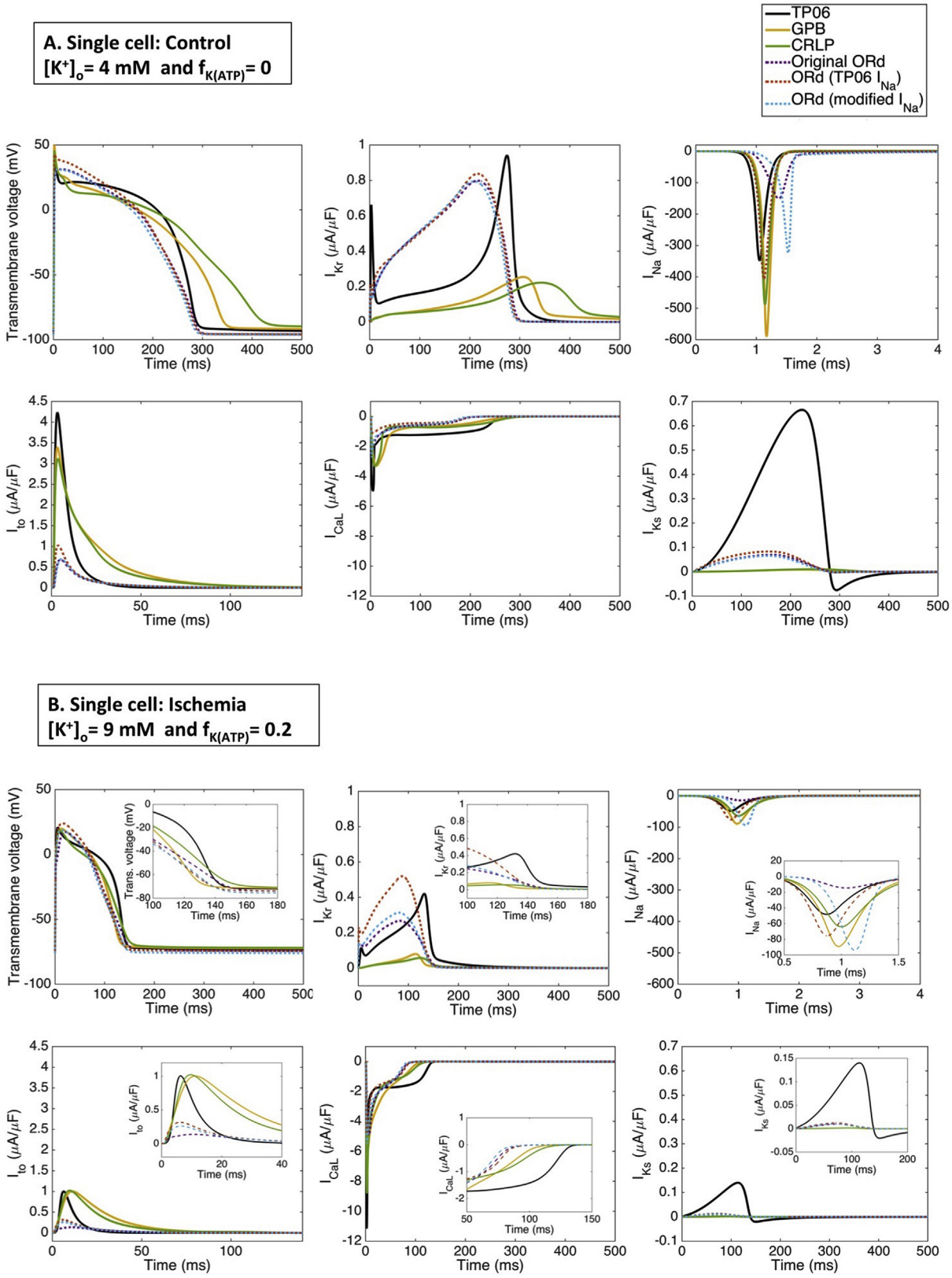

Fig. 1. Action potential (AP), slow (I_{Ks}) and rapid (I_{Kr}) delayed rectifier potassium current, L-type calcium current (I_{CaL}), peak sodium current (I_{Na}) and transient outward potassium current (I_{to}) traces in single cell under (A.) control ($[K^+]_o = 4$ mM; $f_{K(ATP)} = 0$) and (B.) ischemic ($[K^+]_o = 9$ mM; $f_{K(ATP)} = 0.2$) conditions for all the models: ten Tusscher (TP06; black solid line), Grandi (GPB; yellow solid line), Carro (CRLP; green solid line), original O'Hara (original ORd; purple dotted line), O'Hara with TP06 I_{Na} (ORd (TP06 I_{Na}); red dotted line) and O'Hara with modified I_{Na} (ORd (modified I_{Na}); blue dotted line). The same x- and y-axis limits were applied for the respective plots in (A.) and (B.); and inset plots were added to (B.).

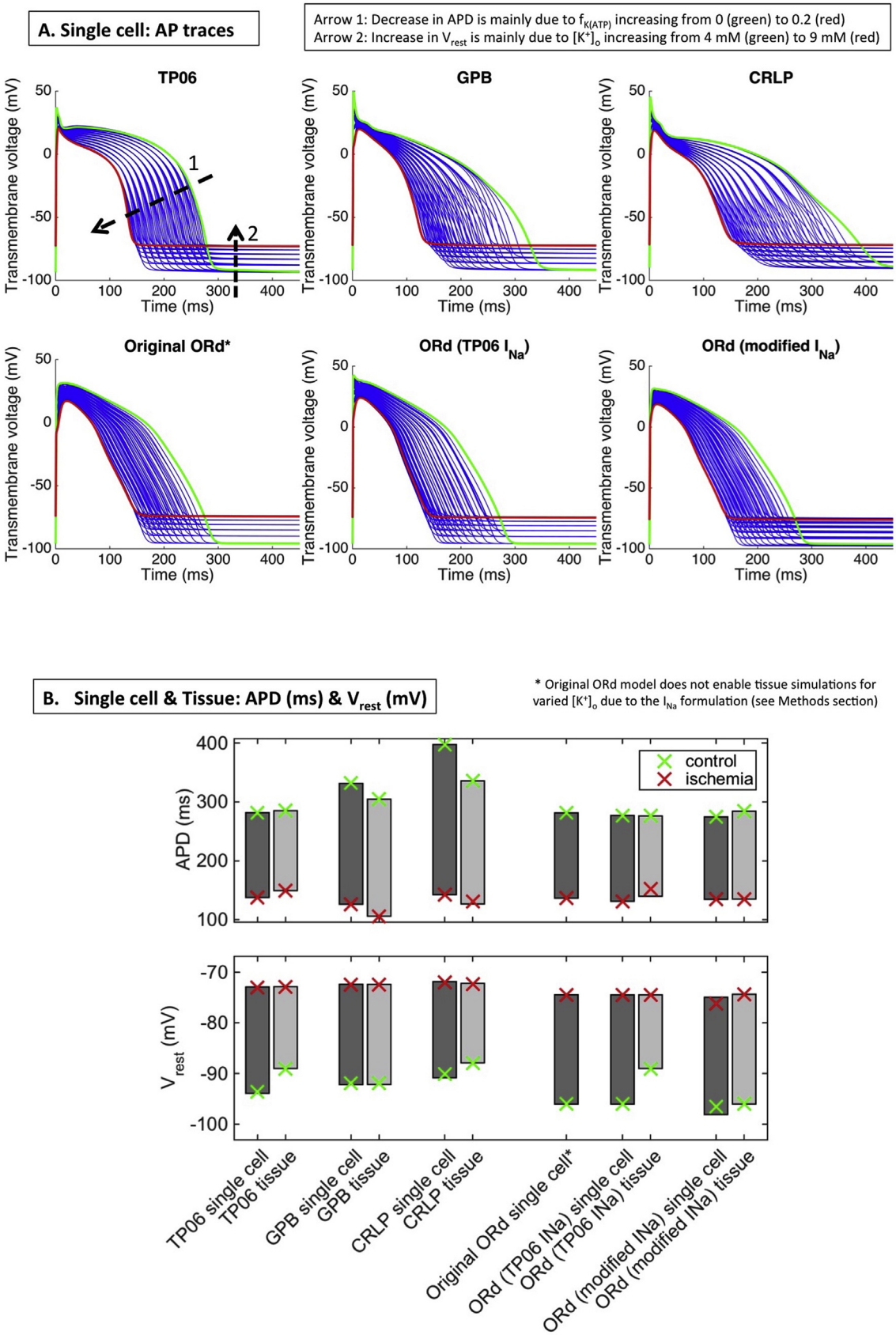

Fig. 2. AP traces (A.) and range of AP duration (APD) and resting membrane potential (V_{rest}) (B.) under varying ischemic conditions ($[K^+]_o$ is varied from 4 to 9 mM; $f_{K(ATP)}$ is varied from 0 to 0.2) in single cell (A.) and both single cell and tissue (B.) for all models. The green AP trace and cross represent control conditions ($[K^+]_o = 4$ mM; $f_{K(ATP)} = 0$) and the red AP trace and cross represent the most ischemic conditions ($[K^+]_o = 9$ mM; $f_{K(ATP)} = 0.2$). In (A.), Arrow 1 emphasizes the decrease in APD mainly due to $f_{K(ATP)}$ increasing from 0 (green) to 0.2 (red). Arrow 2 emphasizes the increase in V_{rest} mainly due to $[K^+]_o$ increasing from 4 mM (green) to 9 mM (red). *Original ORd model does not enable tissue simulations for varied $[K^+]_o$ due to the I_{Na} formulation (see Methods).

3.2. APD and resting membrane potential under varying ischemic conditions

Figs. 2 and 3 show AP morphology, APD, and V_{rest} for all models under varying ischemic conditions ($[K^+]_o$ is varied from 4 to 9 mM; $f_{K(ATP)}$ is varied from 0 to 0.2) in both single cell (Fig. 2) and tissue (Fig. 3). As is shown in Figs. 2A and 3A, all models produce slightly different AP morphologies due to their different ionic formulations. As in single cell, the GPB and CRLP models have a longer control APD than the other models in tissue: 304 and 335 ms for the GPB and CRLP models vs approximately 280 ± 5 ms for the other models. In contrast, in single cell and tissue the differences in APD between the original ORd, the ORd (TP06 I_{Na}), and the ORd (modified I_{Na}) models are small (less than 8 ms), except for the ORd (TP06 INa) model, which displays a 16 ms longer APD under tissue ischemic conditions compared to the other models.

All models produce the expected changes in AP morphology under ischemic conditions: a decrease in APD (such as 282 to 138 ms for the TP06 model in single cell) and a less negative resting membrane potential (V_{rest}) (such as −93 to −73 mV for the TP06 model in single cell). Furthermore, as shown in Fig. 3B, APD decreases as $[K^+]_o$ and $f_{K(ATP)}$ increase. However, the amount of change is different between the models. In fact, the GPB and CRLP models show the biggest change in APD between the control and the ischemic conditions (both in single cell and tissue simulations; as shown in Fig. 2B, single cell APD decreases by 51% and 53% for TP06 and ORd (TP06 I_{Na}) models vs 61% and 64% for GPB and CRLP models). This difference is due to the smaller repolarizing currents in the GPB and CRLP models (i.e., I_{Kr} and I_{Ks}, as shown in Fig. 1), so that the same amount of $I_{K(ATP)}$ current has a larger effect in the GPB and CRLP models than in the other models.

3.3. PRR under varying ischemic conditions

Fig. 4 shows the PRR under varying $[K^+]_o$ and $f_{K(ATP)}$ ischemic conditions for all models both in single cell and tissue, along with the activation and inactivation gates of I_{Na} in single cell. As is shown in Fig. 4, PRR is close to 0 in all cases for $[K^+]_o < 7$ mM, and as the ischemic conditions become more pronounced, PRR increases. Furthermore, PRR is more sensitive to $[K^+]_o$ than $f_{K(ATP)}$, due to its increased effects on the excitability of the cell (Carmeliet, 1999; Janse and Wit, 1989). Nonetheless, the greatest PRR for all models (apart from the original ORd and ORd (TP06 I_{Na}) models in tissue) occurs at the most pronounced ischemic conditions (marked with a red cross in Fig. 4A and 4B) with $[K^+]_o = 9$ mM and $f_{K(ATP)} = 0.2$ (in single cell TP06: 75 ms; GPB: 104 ms; CRLP: 115 ms; ORd (TP06 I_{Na}): 82 ms; ORd (modified I_{Na}): 49 ms). In Fig. 4B, we notice that ischemic conditions in the ORd (TP06 I_{Na}) tissue model (represented by the red cross) do not result in the greatest PRR compared to the maximum PRR observed for $[K^+]_o = 9$ mM and $f_{K(ATP)} = 0$ (82 vs 160 ms, respectively); therefore, PRR for the ORd (TP06 I_{Na}) model is more sensitive to changes in $f_{K(ATP)}$ than for the other models.

As for APD, the amount of change in PRR induced by ischemia

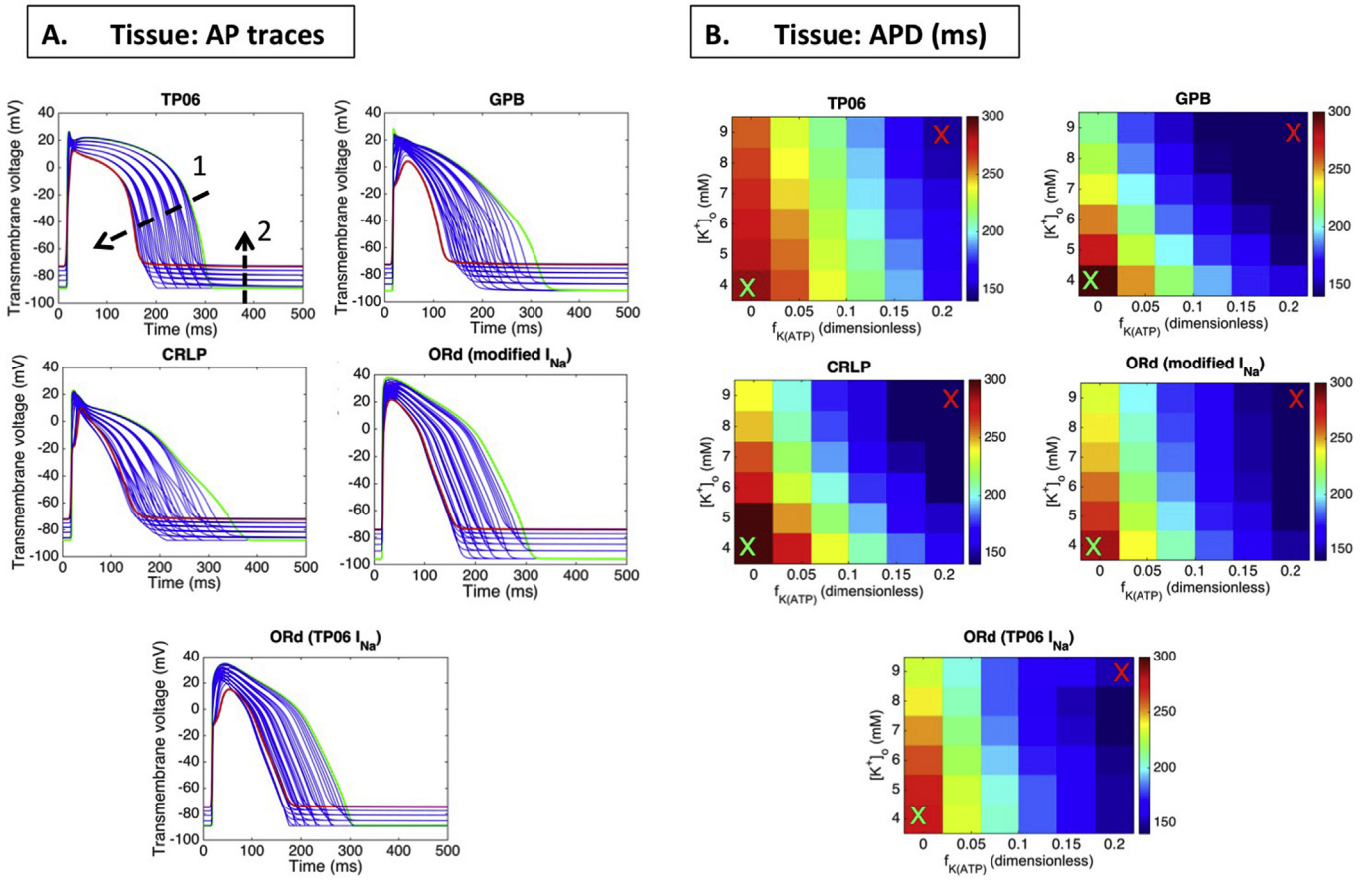

Fig. 3. Tissue AP traces (A.) and APD (B.) under varying ischemic conditions ($[K^+]_o$ is varied from 4 to 9 mM; $f_{K(ATP)}$ is varied from 0 to 0.2) for all models. The green AP trace and cross represent control conditions ($[K^+]_o = 4$ mM; $f_{K(ATP)} = 0$) and the red AP trace and cross represent the most ischemic conditions ($[K^+]_o = 9$ mM; $f_{K(ATP)} = 0.2$). Arrows and * as in Fig. 2.

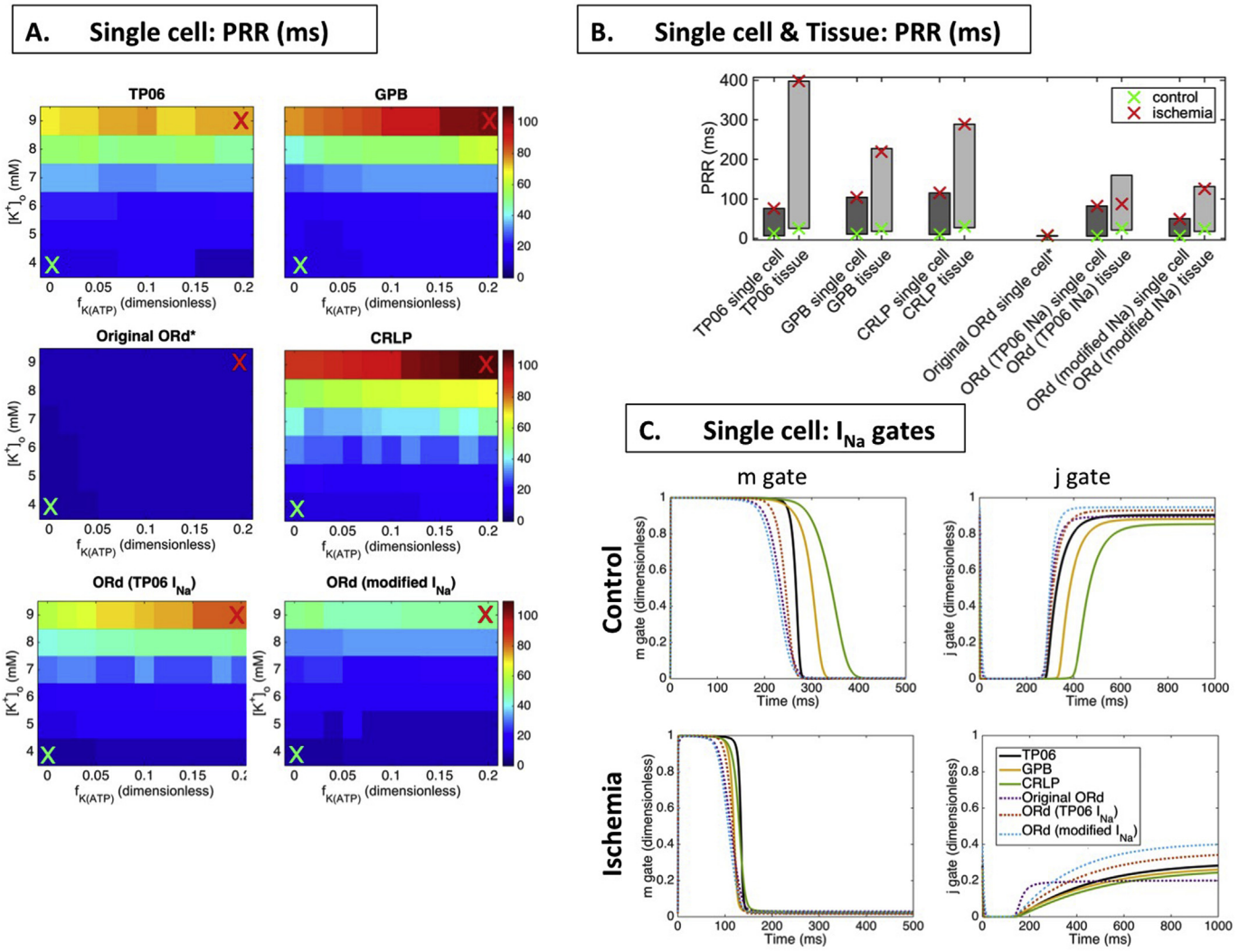

Fig. 4. Post-repolarization refractoriness (PRR) in single cell (A.) and range of PRR in both single cell and tissue (B.) for all models under varying ischemic conditions. The green and red crosses represent control ($[K^+]_o$ = 4 mM; $f_{K(ATP)} = 0$) and ischemic conditions ($[K^+]_o$ = 9 mM; $f_{K(ATP)} = 0.2$). (C.) Activation (m gate) and inactivation (j gate) gates of I_{Na} under control and ischemic conditions for all the models (as in Fig. 1). *(as in Fig. 2).

varies from model to model. The TP06, GPB and CRLP models show the greatest increase in PRR, due to a delayed recovery of the I_{Na} current (Fig. 4C), as the activation and inactivation gates recover later and reach a lower steady state than in the other models (apart from the original ORd model). The original ORd model, on the other hand, does not display an increase in PRR in single cell and does not propagate activation in tissue with increased $[K^+]_o$. This is due to a faster recovery and lower steady state of the I_{Na} inactivation gates (Fig. 4C) than in other models under ischemic conditions. This is improved in the ORd (TP06 I_{Na}) and ORd (modified I_{Na}) models; under ischemic conditions the h and j gate steady state value is higher and slower than the original ORd (Fig. 4C), hence, those models reproduce the expected increase in PRR. However, the change is smaller than in the TP06, GPB and CRLP models due to a faster recovery of the activation and inactivation I_{Na} gates.

In addition, Fig. 4B shows that PRR in tissue is more pronounced than in single cell. This is due primarily to differences in the method for calculation of ERP between single cell and tissue simulations. In the tissue simulations, the extra stimulus must be strong enough to trigger a wave of activation that will reach the end of the 5 cm strand of tissue to be counted as successful, while in single cells the stimulus only needs to be strong enough to activate a single cell. Furthermore, studies have shown that differences between single cell and tissue occur due to cell coupling via gap junctions, for example specific conditions are needed in tissue for a single cell's activation to propagate to the neighboring tissue (Joyner et al., 1991; Xie et al., 2010).

3.4. CV, upstroke velocity and peak voltage under varying ischemic conditions

Fig. 5 shows CV, dV/dt_{max}, and peak V_m (V_{max}) under varying ischemic conditions for all models in single cell and tissue (apart from CV that is calculated in tissue only). Fig. 5A shows that CV, under control conditions, is similar in all models (0.067, 0.077, 0.074, 0.069 and 0.059 cm/ms for the TP06, GPB, CRLP, ORd (TP06 I_{Na}) and ORd (modified I_{Na}) models). However, the ORd (modified I_{Na}) model displays smaller changes in CV during ischemia (0.15 vs 0.4 cm/ms for the TP06, GPB and CRLP models). Fig. 5A also shows that CV becomes slower as $[K^+]_o$ increases, due to reduced I_{Na} availability caused by a less negative resting potential. However, CV is unchanged with variations of $f_{K(ATP)}$, as the repolarizing current $I_{K(ATP)}$ primarily affects repolarization.

Fig. 5B shows that dV/dt_{max} and V_{max} are decreased in all models

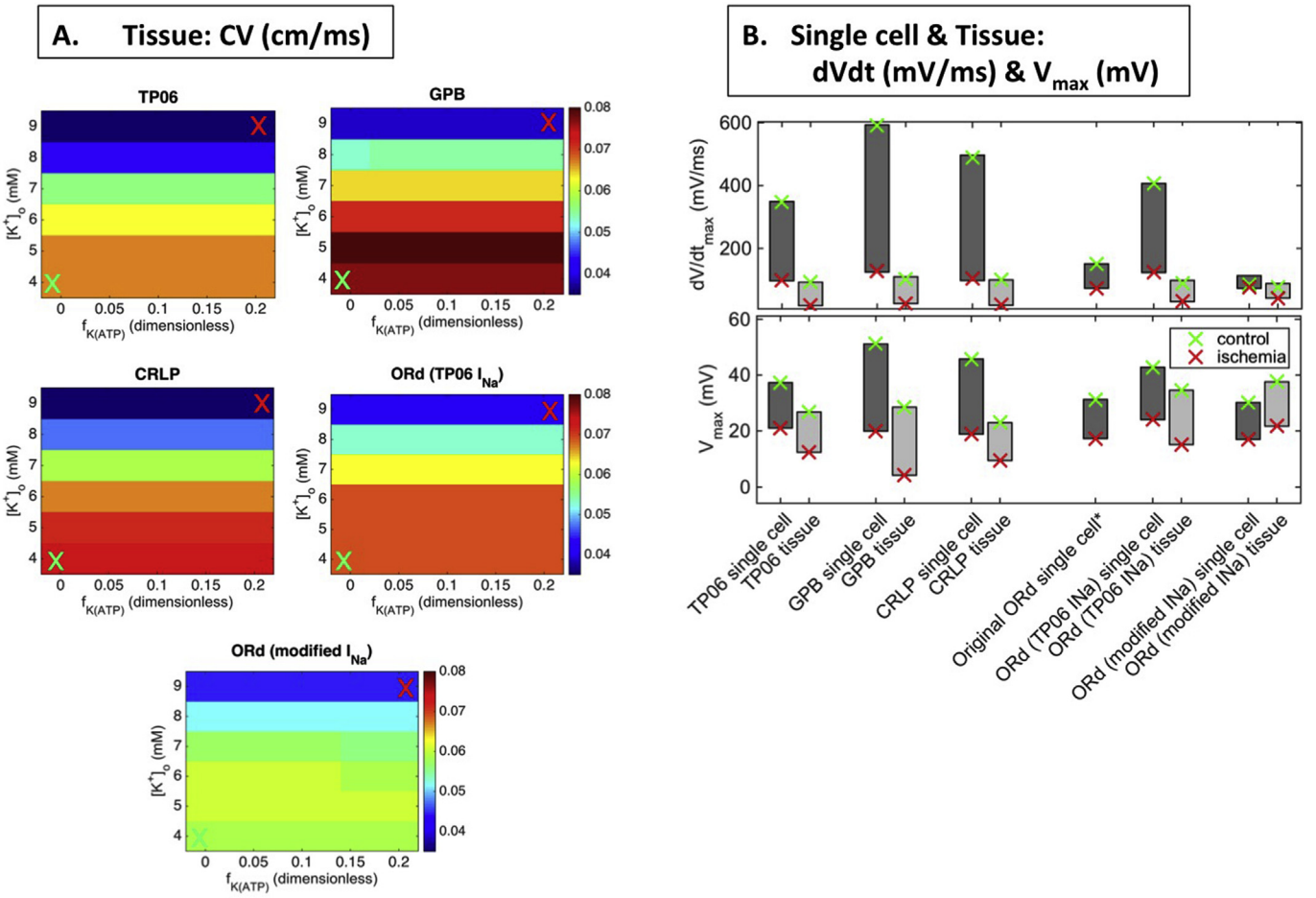

Fig. 5. Conduction velocity (CV) in tissue (A.) and range of maximum upstroke velocity (dV/dt_{max}) and maximum transmembrane voltage (V_{max}) in both single cell and tissue (B.) for all models under varying ischemic conditions. The green and red crosses represent control ($[K^+]_o = 4$ mM; $f_{K(ATP)} = 0$) and ischemic conditions ($[K^+]_o = 9$ mM; $f_{K(ATP)} = 0.2$). *(as in Fig. 2).

for the most ischemic conditions (red cross). For example, TP06 single cell dV/dt_{max} decreases from 348.5 to 98.9 mV/ms between control and ischemic conditions (green and red cross). Both of these properties are also affected primarily by $[K^+]_o$, showing little to no change for varying $f_{K(ATP)}$ (data not shown). We notice that the original ORd and ORd (modified I_{Na}) models display a smaller dV/dt_{max} than the other models due to a smaller I_{Na} current (Fig. 1).

Both dV/dt_{max} and V_{max} for the TP06, GPB, CRLP and ORd (TP06 I_{Na}) models show greater values in single cell than in tissue, due to the stimulus current being applied directly to the cell in the single cell simulations, while in tissue the stimulus comes from the excitation of the neighboring cells. Nonetheless, both in single cell and tissue, the models reproduce the expected ischemic changes: a decrease in dV/dt_{max} and V_{max}.

3.5. APD and CV restitution curves under control and ischemic conditions

Fig. 6 shows CV and APD restitution curves for all models under control ($[K^+]_o = 4$ mM and $f_{K(ATP)} = 0$) and ischemic conditions ($[K^+]_o = 9$ mM and $f_{K(ATP)} = 0.2$). We notice that overall, under ischemic conditions, the restitution curves are flattened (for example TP06 APD restitution slope is decreased from 0.559 in control to 0.015 in ischemia), as shown experimentally (Kurz et al., 1994). In fact, the TP06 and ORd (modified I_{Na}) models display the flattest APD restitution curve under ischemic conditions, with no change in APD for varying diastolic intervals. On the other hand, the ORd (TP06 I_{Na}) and GPB models do not display the expected flattening in APD restitution and show a slight increase in slope, while the CRLP model displays alternans for shorter diastolic intervals, as observed experimentally (Kurz et al., 1994). However, for the CV restitution curves under ischemic conditions, the GPB model displays the flattest restitution curve, and all other models show a slight decrease in CV for decreasing cycle length.

3.6. Comparison to experimental data

Table 1 summarizes ischemia-induced changes in electrophysiological properties (APD, PRR, CV, V_{rest}, AP amplitude (APA) and dV/dt_{max}) in clinical human and experimental animal studies. Sutton et al. and Taggart et al. investigated effects of occlusion of the left anterior descending artery for 3 min in patients while they were undergoing open chest surgery for two different stimuli (Sutton et al., 2000; Taggart, 2000). While Kodama et al., Penny et al., and Kimura et al. investigated the effects of simulated ischemia in *in vitro* guinea pig and cat for 10 and 15 min of ischemia (Kimura et al., 1990; Kodama et al., 1984; Penny and Sheridan, 1983). Many more ischemia experimental animal studies exist; however, these three studies present a degree of ischemia and corresponding changes in biomarkers that are similar to the ones investigated in our study.

When comparing simulation results to Sutton et al. and Taggart

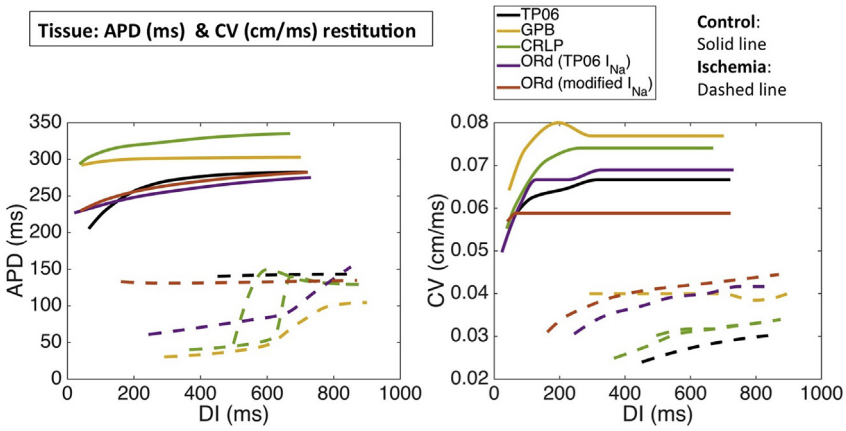

Fig. 6. APD and CV restitution curves in tissue for all models (apart from the original ORd*; TP06 in black, GPB in yellow, CRLP in green, ORd (TP06 I_{Na}) in purple and ORd (modified I_{Na}) in red) under control (solid line) and ischemic conditions (dashed line) for varying diastolic intervals (DI). The CRLP model displays alternans for shorter DIs under ischemic conditions. *(as in Fig. 2).

Table 1
Summary of ischemia-induced changes in electrophysiological properties (action potential duration (APD), post-repolarization refractoriness (PRR), conduction velocity (CV), resting membrane potential (V_{rest}), action potential amplitude (APA) and maximum upstroke velocity (dV/dt_{max})) in clinical and experimental studies (Kimura et al., 1990; Kodama et al., 1984; Penny and Sheridan, 1983; Sutton et al., 2000; Taggart, 2000). Sutton et al. present changes for two different stimuli (two times diastolic threshold/four times diastolic threshold). Taggart et al. present changes for transmural/longitudinal CV. Kodama et al., Penny et al. and Kimura et al. present changes for 10/15 min of ischemia.

References	[Sutton et al.]	[Taggart et al.]	[Kodama et al.]	[Penny et al.]	[Kimura et al.]
Species	Human	Human	Guinea-pig	Guinea-pig	Cat
Preparation Type	In vivo whole heart	In vivo whole heart	Isolated papillary muscle	In vitro whole heart	Isolated myocytes
Recording type	surface electrodes	plunge electrodes	micro-electrodes	electrocardiogram	micro-electrodes
Changes observed	ΔAPD: 60/70 ms ΔPRR: 62/150 ms	ΔCV: 10/18 cm/s	ΔAPD: 74/90 ms ΔV_{rest}: 11/12 mV ΔAPA: 30/34 mV $\Delta dVdt_{max}$: 210/205 mV/ms	ΔAPD: 45/65 ms ΔAPA: 25/35 mV $\Delta dVdt_{max}$: 80/80 mV/ms	ΔAPD: 40/55 ms ΔV_{rest}: 20/25 mV ΔAPA: 25/30 mV
Time of Ischemia	3 min	3 min	10/15 min	10/15 min	10/15 min
Notes	2 types of stimulus: 4 times and 2 times control diastolic threshold	Calculated transmural and longitudinal CV	Altered extracellular solution (10 mM $[K^+]_o$ and acidic environment)	Zero flow ischemia (langendorff perfusion system)	Altered extracellular solution to mimic ischemia

et al., a value of $[K^+]_o = 7$ mM (as in (Vermeulen, 1996)) and $f_{K(ATP)} = 0.08$ (as in (Moréna et al., 1980)) was chosen to reproduce 3 min of ischemia. Table 2 summarizes changes in APD, PRR, and CV between control ($[K^+]_o = 4$ mM and $f_{K(ATP)} = 0$) and 3 min of ischemia ($[K^+]_o = 7$ mM and $f_{K(ATP)} = 0.08$) for all models in single cell and tissue simulations. We notice that the TP06 model displays the closest change in APD to experimental data (60 ms in single cell and 65 ms in tissue), while the GPB and CRLP models show more than double the change in APD observed experimentally. Nonetheless, all models show a much smaller increase in PRR than the one observed experimentally, apart for the TP06 model in tissue that shows a 62 ms increase in PRR. Finally, the TP06, GPB and CRLP models show a change in CV that is in line with experimental data. Therefore, overall the TP06 model shows best agreement with experimental data from human after 3 min of ischemia, although the PRR change in single cell is lower.

Table 2
Summary of ischemia-induced changes in APD, PRR and CV between control ($[K^+]_o = 4$ mM and $f_{K(ATP)} = 0$) and after 3 min of ischemia ($[K^+]_o = 7$ mM and $f_{K(ATP)} = 0.08$) in single cell/tissue simulations for the ten Tusscher (TP06), modified Grandi (GPB), Carro (CRLP), original O'Hara (original ORd), and two modified I_{Na} ORd models (ORd (TP06 I_{Na}) and ORd (modified I_{Na})).

After 3 min of ischemia	ΔAPD (ms)	ΔPRR (ms)	ΔCV (cm/s)
TP06	66/65	20/62	11.1
GPB	142/132	21/37	12.4
CRLP	167/148	27/48	16
original ORd	100/NA	0/NA	NA
ORd (TP06 I_{Na})	99/93	20/33	6.46
ORd (modified I_{Na})	88/101	14/35	1.7

Experimental results in animal models after 10 and 15 min of ischemia were compared to simulation results with $[K^+]_o = 9$ mM and $f_{K(ATP)} = 0.2$ set as the ischemic conditions (see Table 3). The change in APD is greater for all models (above 144 ms) than in the animal studies (90 ms maximum); however, if we take the % decrease in APD both the experimental and the simulation results show approximately a 40–50% decrease in APD (results not shown). The increase in V_{rest} observed experimentally is between 11 and 25 mV, and all the models show changes within that range. The same was observed for AP amplitude, apart from the GPB model, which shows a bigger change of 51 and 44 mV in single cell and tissue, respectively. Finally, a wide range of values are observed experimentally for the change in dV/dt_{max}, ranging from 80 to 210 mV/ms. The GPB, CRLP and ORd (modified I_{Na}) models show values that are greater (up to 463 mV/ms in single cell for the GPB model). The ORd (TP06 I_{Na}) model shows a particularly low value for both single cell and tissue of 8 and 35 mV/ms respectively. The rest of the tissue simulations also show a slightly lower change in dV/dt_{max} (like the ORd (modified I_{Na}), TP06, and GPB models). Therefore, overall, the TP06, CRLP, and ORd (modified I_{Na}) models show good agreement with guinea-pig and cat experimental data, apart from dV/dt_{max}.

Table 3
Summary of ischemia-induced changes in APD, PRR, CV, V_{rest}, APA and dV/dt_{max} between control ($[K^+]_o = 4$ mM and $f_{K(ATP)} = 0$) and after 10 min of ischemia ($[K^+]_o = 9$ mM and $f_{K(ATP)} = 0.2$) in single cell/tissue simulations for all models (as in Table 2).

After 10 min of ischemia	ΔAPD (ms)	ΔPRR (ms)	ΔCV (cm/s)	ΔV_{rest} (mV)	ΔAPA (mV)	$\Delta dV/dt_{max}$ (mV/ms)
TP06	144/136	63/372	37	20/17	37/30	249/73
GPB	205/199	93/196	41	19/19	51/44	463/77
CRLP	255/204	105/259	41	18/15	45/29	385/80
original ORd	144	0	N/A	22	36	78
ORd (modified I_{Na})	146/124	76/61	57	22/15	33/38	283/58
ORd (TP06 I_{Na})	142/149	43/102	16	20/22	40/34	8/35

4. Discussion

This study investigates the behavior of recent human models under control and varying ischemic conditions by evaluating various electrophysiological properties related to arrhythmic risk (such as APD, PRR and CV) in single cell and tissue, and comparing them to available experimental data. Furthermore, our study is the first to introduce adaptations of the ORd (with a modified I_{Na} current) and the GPB (with a modified $[K^+]_i$) models, which can reproduce expected ischemia-induced changes. With the alternative formulations, all models tested reproduce ischemia-induced changes in APD (decrease), V_{rest} (less negative), PRR (increase), CV (slower), dV/dt_{max} (decrease), V_{max} (decrease), and restitution curves (flattening; apart from the GPB and ORd (TP06 I_{Na}) that do not show APD restitution curve flattening), in line with experimental data (Carmeliet, 1999; Coronel et al., 2012; Janse and Wit, 1989; Sutton et al., 2000; Taggart, 2000; Vermeulen, 1996; Watanabe et al., 1997; Wilensky et al., 1986). Dispersion of these properties between the ischemic and normal tissue is critical for investigations of arrhythmogenesis during ischemia, as they play an important role in triggering and sustaining arrhythmias (Janse and Wit, 1989; Nademanee et al., 1985; Zaitsev et al., 2003). To the best of our knowledge, this is the first systematic comparison of these human ventricular AP models under ischemic conditions, which extends our previous study (Dutta et al., 2013), also yielding adaptations of the ORd and the GPB models for evaluation of ischemic conditions. Furthermore, we show the importance of assessing various electrophysiological markers (as limitations of the original ORd are not apparent if one only measures APD), as well as performing both single cell and tissue simulations (the original ORd does not show propagation of excitation in tissue with hyperkalemia).

4.1. All models reproduce ischemia-induced changes

Both the single cell and tissue results show that all models reproduce the expected ischemic APD behavior (Figs. 2–4). As $[K^+]_o$ and peak $I_{K(ATP)}$ increase, APD becomes shorter, with the shortest APD occurring for the highest values of $[K^+]_o$ and peak $I_{K(ATP)}$ (Fig. 3). The increased peak $I_{K(ATP)}$ current accelerates the repolarization process due to an increased outward flux of K^+ ions; therefore, decreasing the APD, as has been shown experimentally (Carmeliet, 1999; Coronel et al., 1988; Furukawa et al., 1991; Pandit et al., 2011; Sutton et al., 2000; Watanabe et al., 1997). Overall, all models show good quantitative agreement to animal studies; even though the GPB and CRLP models show more than double the change in APD observed clinically after 3 min of ischemia (see Section 3.5).

Both the single cell and tissue results show that all models (except for the original ORd) reproduce an increase in PRR as $[K^+]_o$ increases (Fig. 4). The longest PRR occurs for the highest values of $[K^+]_o$ and peak $I_{K(ATP)}$. Experimental data has shown that PRR increases significantly under ischemic conditions, as is described in the review by Coronel et al. (2012). and in the clinical studies carried out by Sutton et al. (2000); however, the increase observed in all models is smaller than the one observed clinically, apart from the TP06 model in tissue (see Section 3.5). As $[K^+]_o$ increases, the resting potential becomes less negative and this reduces sodium channel availability, thus decreasing the cell's excitability, as has been described by Taggart et al. (Taggart and Slater, 1971). In all models, the PRR is more sensitive to changes in $[K^+]_o$ than changes in peak $I_{K(ATP)}$ conductance, as $[K^+]_o$ has a greater effect on cell excitability.

As shown in Fig. 5, CV is significantly slower for high values of $[K^+]_o$, reaching values close to 0.03 cm/ms. Our results shows that CV is more sensitive to $[K^+]_o$ than to the repolarizing current $I_{K(ATP)}$; this is expected, as CV is not directly affected by repolarization. Such differences in CV between normal and ischemic tissue often lead to conduction block and reentry due to heterogeneities in tissue activation (Carmeliet, 1999; Dutta et al., 2016; Janse et al., 1980; Tice et al., 2007). Our results are in agreement with human data from Taggart et al. that show CV control values ranging from 0.05 to just under 0.07 cm/ms, and ischemic values of 0.027 cm/ms (Taggart, 2000), apart from the two modified ORd models that show a smaller change in CV.

Finally, dV/dt_{max} and V_{max} also decrease as $[K^+]_o$ increases, as shown experimentally (Kleber, 1983), and most models reproduce a flattening of the APD and CV restitution curves during ischemia, as shown experimentally (Kurz et al., 1994), apart from the GPB and ORd (TP06 I_{Na}) models, which do not display APD restitution flattening.

As described above, the models qualitatively reproduce the expected ischemia-induced changes (a decrease in APD and CV and an increase in PRR), but in some cases they show quantitative differences. For example, the effect of varying peak $I_{K(ATP)}$ conductance on APD (Figs. 2–4) is more pronounced in the GPB and CRLP models compared to the other models (Fig. 1) and experimental data (Section 3.5), due to the decreased amplitudes of the repolarizing currents I_{Kr} and I_{Ks}. Moreover, the TP06, CRLP, and GPB models show the greatest change in PRR and CV between control and ischemic conditions due to the gating properties of I_{Na} (Figs. 4 and 6). Finally, the TP06 model shows the greatest change in its APD restitution curve between control and ischemic conditions, while with ischemia the GPB model shows the greatest change in its CV restitution curve and the CRLP model shows AP alternans, which has been reported experimentally, but is difficult to detect clinically in human (Kurz et al., 1994, 1993; Nakashima et al., 1978). These differences may be important for determining the choice of human model for simulations of ischemia.

Interestingly, while the 3 ORd model versions show similar AP morphology, APD, and V_{rest} under varying ischemic conditions (Figs. 1 and 2), differences exist for PRR (Fig. 4) and dV/dt_{max} (Fig. 5B), where I_{Na} plays a bigger role. The original ORd formulation does not reproduce an increase in PRR and does not propagate excitation in tissue under ischemic conditions. However, both modified versions of the model do reproduce the expected increase

in PRR, although it remains lower than in the TP06, CRLP, and GPB models.

4.2. Comparison between experimental and simulation data

To the best of our knowledge, only Sutton et al. and Taggart et al. present electrophysiological recordings of ischemia on human tissue, and report shortening of APD (by 60 ms) and PRR (by 62 ms), and a decrease in CV (by 10–18 cm/s) following 3 min of coronary occlusion (Sutton et al., 2000; Taggart, 2000). This is consistent with the data obtained by Kodama et al., Penny et al., and Kimura et al. in guinea pig and cat experiments (Kimura et al., 1990; Kodama et al., 1984; Penny and Sheridan, 1983). The models tested in the present study show good agreement with the experimental data, particularly the TP06 and ORd (modified I_{Na}) models.

The experimental/computational data comparison, however, must be interpreted in light of the following considerations. Firstly, acute ischemia is a dynamic process both spatially and temporally, as shown in a variety of studies and animal species (Carmeliet, 1999; Schaapherder et al., 1990; Vermeulen, 1996; Wilde et al., 1990; Wilensky et al., 1986). The time course of the ischemia-induced alterations is affected by the severity of the lack of flow, as well as other possible factors such as the metabolic state of the tissue prior to the onset of ischemia, the specific ion channel densities in each cell (Gemmell et al., 2016), or the level of ischemic preconditioning (Carmeliet, 1999). It is therefore very likely that the course and severity of electrophysiological changes during acute ischemia in the human population would be variable. Therefore, the data available provide a valuable, but limited snapshot of the electrophysiological consequences of ischemia in the human population.

Secondly, reproducing acute ischemic conditions experimentally is challenging and likely to be greatly influenced by the experimental set up itself. Indeed, measurements during open chest surgery or in isolated hearts, for instance, are likely to be influenced by possible changes in temperature, that are known to lead to an increase in APD (Lab and Woollard, 1978). Furthermore, an important component of acute ischemia is the lack of flow, and hence washout, which enables the extracellular accumulation of potassium; this cannot be easily reproduced (even using mini-wells designed for this purpose), so often solutions mimicking the ischemic changes are used (Kimura et al., 1990; Kodama et al., 1984).

Electrophysiological recordings in acute ischemia and their comparison to simulation results need to be interpreted taking into account these factors (i.e. the dynamic nature of ischemia and the limitations of reproducing these changes experimentally), as well as the importance of evaluating the consistency of the model-simulation-experiment system (Carusi et al., 2012; Quinn and Kohl, 2013). Therefore, in this study, we evaluate and enhance the ability of the human ventricular models to reproduce the well-established electrophysiological alterations of acute ischemia including APD shortening, increased post-repolarization refractoriness, and slow conduction, recorded in human as well as in animal studies. The time course and severity of ischemic changes in human is likely to be very variable and only a limited set of recordings is available, which is within range of the changes shown in the simulations.

5. Conclusions

In this paper, a systematic analysis is performed to investigate the use of recent human AP models for studies of ischemia. The results present the sensitivity of some important arrhythmic electrophysiological parameters (APD, PRR, and CV) to variations in two primary ischemic parameters (an increase in $[K^+]_o$ and peak $I_{K(ATP)}$) in recent human ventricular AP models (TP06, GPB with a modified intracellular potassium concentration, CRLP, ORd, and two versions of ORd with modified I_{Na} current) using single cell and tissue simulations. We show that all the models (after changes to the GPB and ORd model) show the expected ischemia-induced changes, in agreement with experimental data.

Previous studies established that the main factors explaining ischemia-induced changes are hyperkalemia, $I_{K(ATP)}$ activation, and inhibition of the I_{Na} and I_{CaL} currents by acidosis. However, both the SERCA and the sodium potassium pump are also compromised in ischemia (Fuller et al., 2003; Terkildsen et al., 2008; Tran et al., 2009). One of the consequences of sodium potassium pump inhibition is the extracellular accumulation of potassium, which is already accounted for in our simulations. However, SERCA is likely to affect calcium dynamics and promote cardiac alternans (Baumeister and Quinn, 2016; Zhou et al., 2016), which should be investigated in future studies.

Overall, results from this study will help in the selection of an appropriate cell model for human-specific simulations of myocardial ischemia, by demonstrating quantitative differences to ischemia-induced changes across the models. This study also highlights the importance of considering multiple measured parameters in both single cell and tissue simulations when assessing the applicability of models for a given simulation. Finally, the authors suggest the ORd (modified I_{Na}) model may be a suitable initial choice for ischemia simulations, given that the original ORd model is based on the latest knowledge of human ventricular cells and these features are mostly unchanged in the ORd (modified I_{Na}) model, while enabling simulations of hyperkalemia.

Acknowledgements

We would like to acknowledge Dr. Bueno-Orovio, Dr. Dangerfield, Prof. Burrage, and the Chaste team for discussions, insight and technical support on the use of the models and their modified versions.

Appendix A. Supplementary data

Supplementary data related to this article can be found at http://dx.doi.org/10.1016/j.pbiomolbio.2017.02.007.

Disclosures

None.

Funding sources

This work was supported by a Wellcome Trust Fellowship in Basic Biomedical Sciences [grant number 100246/Z/12/Z to B.R.], an Engineering and Physical Sciences Research Council doctoral scholarship [EPSRC ref: EP/G03706X/1 to S.D.], a Marie Curie Intra-European fellowship for Career Development [to A.M.], a Heart and Stroke Foundation of Canada National New Investigator Award [to T.A.Q.], and the Canadian Institutes of Health Research [MOP 142424 to T.A.Q.] and Nova Scotia Health Research Foundation [MED-EST-2014-9582 to T.A.Q.].

References

Baumeister, P.A., Quinn, T.A., 2016. Altered Calcium Handling and Ventricular Arrhythmias in Acute Ischemia. Clin. Med. Insights Cardiol. 10, 61–69. http://dx.doi.org/10.4137/CMC.S39706.

Bernabeu, M.O., Southern, J., Wilson, N., Strazdins, P., Cooper, J., Pitt-Francis, J., 2014. Chaste. Int. J. High. Perform. Comput. Appl. 28, 13–32. http://dx.doi.org/10.1177/

1094342012474997.
Bernus, O., Wellner, M., Mironov, S.F., Pertsov, A.M., 2005. Simulation of voltage-sensitive optical signals in three-dimensional slabs of cardiac tissue: application to transillumination and coaxial imaging methods. Phys. Med. Biol. 50, 215+. http://dx.doi.org/10.1088/0031-9155/50/2/003.
Carmeliet, E., 1999. Cardiac ionic currents and acute ischemia: from channels to arrhythmias. Physiol. Rev. 79, 917–1017.
Carro, J., Rodríguez, J.F., Laguna, P., Pueyo, E., 2011. A human ventricular cell model for investigation of cardiac arrhythmias under hyperkalaemic conditions. Philos. Trans. R. Soc. Math. Phys. Eng. Sci. 369, 4205–4232. http://dx.doi.org/10.1098/rsta.2011.0127.
Carusi, A., Burrage, K., Rodríguez, B., 2012. Bridging experiments, models and simulations: an integrative approach to validation in computational cardiac electrophysiology. Am. J. Physiol. - Heart Circ. Physiol. 303, H144–H155. http://dx.doi.org/10.1152/ajpheart.01151.2011.
Cherry, E.M., Fenton, F.H., 2007. A tale of two dogs: analyzing two models of canine ventricular electrophysiology. Am. J. Physiol. - Heart Circ. Physiol. 292, H43–H55. http://dx.doi.org/10.1152/ajpheart.00955.2006.
Coronel, R., 1994. Heterogeneity in extracellular potassium concentration during early myocardial ischaemia and reperfusion: implications for arrhythmogenesis. Cardiovasc. Res. 28, 770–777. http://dx.doi.org/10.1093/cvr/28.6.770.
Coronel, R., Fiolet, J.W., Wilms-Schopman, F.J., Schaapherder, A.F., Johnson, T.A., Gettes, L.S., Janse, M.J., 1988. Distribution of extracellular potassium and its relation to electrophysiologic changes during acute myocardial ischemia in the isolated perfused porcine heart. Circulation 77, 1125–1138.
Coronel, R., Janse, M.J., Opthof, T., Wilde, A.A., Taggart, P., 2012. Postrepolarization refractoriness in acute ischemia and after antiarrhythmic drug administration: action potential duration is not always an index of the refractory period. Heart Rhythm Off. J. Heart Rhythm Soc. 9, 977–982. http://dx.doi.org/10.1016/j.hrthm.2012.01.021.
Coronel, R., Wilms-Schopman, F.J., Opthof, T., van Capelle, F.J., Janse, M.J., 1991. Injury current and gradients of diastolic stimulation threshold, TQ potential, and extracellular potassium concentration during acute regional ischemia in the isolated perfused pig heart. Circ. Res. 68, 1241–1249.
Dutta, S., Minchole, A., Quinn, T.A., Rodriguez, B., 2013. Recent human ventricular cell action potential models under varied ischaemic conditions. In: Computing in Cardiology Conference (CinC), 2013. IEEE, pp. 695–698.
Dutta, S., Mincholé, A., Zacur, E., Quinn, T.A., Taggart, P., Rodriguez, B., 2016. Early afterdepolarizations promote transmural reentry in ischemic human ventricles with reduced repolarization reserve. Prog. Biophys. Mol. Biol. 120, 236–248. http://dx.doi.org/10.1016/j.pbiomolbio.2016.01.008.
Elshrif, M.M., Cherry, E.M., 2014. A quantitative comparison of the behavior of human ventricular cardiac electrophysiology models in tissue. PLoS ONE 9, e84401+. http://dx.doi.org/10.1371/journal.pone.0084401.
Ferrero, J.M., Sáiz, J., Ferrero, J.M., Thakor, N.V., 1996. Simulation of action potentials from metabolically impaired cardiac myocytes. Circ. Res. 79, 208–221. http://dx.doi.org/10.1161/01.res.79.2.208.
Fiolet, J., Baartscheer, A., Schumacher, C., Terwelle, H., Krieger, W., 1985. Transmural inhomogeneity of energy metabolism during acute global ischemia in the isolated rat heart: dependence on environmental conditions. J. Mol. Cell. Cardiol. 17, 87–92. http://dx.doi.org/10.1016/s0022-2828(85)80095-x.
Fuller, W., Parmar, V., Eaton, P., Bell, J.R., Shattock, M.J., 2003. Cardiac ischemia causes inhibition of the Na/K ATPase by a labile cytosolic compound whose production is linked to oxidant stress. Cardiovasc. Res. 57, 1044–1051. http://dx.doi.org/10.1016/s0008-6363(02)00810-6.
Furukawa, T., Kimura, S., Furukawa, N., Bassett, A.L., Myerburg, R.J., 1991. Role of cardiac ATP-regulated potassium channels in differential responses of endocardial and epicardial cells to ischemia. Circ. Res. 68, 1693–1702.
Garny, A., Kohl, P., Noble, D., 2003. Cellular open resource (COR): a public cellml based environment for modeling biological function. Int. J. Bifurc. Chaos 13, 3579–3590. http://dx.doi.org/10.1142/s021812740300882x.
Gemmell, P., Burrage, K., Rodríguez, B., Quinn, T.A., 2016. Rabbit-specific computational modelling of ventricular cell electrophysiology: using populations of models to explore variability in the response to ischemia. Prog. Biophys. Mol. Biol. 121, 169–184. http://dx.doi.org/10.1016/j.pbiomolbio.2016.06.003.
Grandi, E., Pasqualini, F.S., Bers, D.M., 2010. A novel computational model of the human ventricular action potential and Ca transient. J. Mol. Cell. Cardiol. 48, 112–121. http://dx.doi.org/10.1016/j.yjmcc.2009.09.019.
Heidenreich, E.A., Ferrero, J.M., Rodríguez, J.F., 2012. Modeling the human heart under acute ischemia. In: Calvo Lopez, B., Pena, E. (Eds.), Patient-Specific Computational Modeling. Springer Netherlands, Dordrecht, pp. 81–103. https://doi.org/10.1007/978-94-007-4552-0_4.
Irisawa, H., Sato, R., 1986. Intra- and extracellular actions of proton on the calcium current of isolated Guinea pig ventricular cells. Circ. Res. 59, 348–355.
Janse, M.J., van Capelle, F.J., Morsink, H., Kléber, A.G., Wilms-Schopman, F., Cardinal, R., d' Alnoncourt, C.N., Durrer, D., 1980. Flow of "injury" current and patterns of excitation during early ventricular arrhythmias in acute regional myocardial ischemia in isolated porcine and canine hearts. Evidence for two different arrhythmogenic mechanisms. Circ. Res. 47, 151–165.
Janse, M.J., Wit, A.L., 1989. Electrophysiological mechanisms of ventricular arrhythmias resulting from myocardial ischemia and infarction. Physiol. Rev. 69, 1049–1169.
Joyner, R.W., Sugiura, H., Tan, R.C., 1991. Unidirectional block between isolated rabbit ventricular cells coupled by a variable resistance. Biophys. J. 60, 1038–1045.
Kazbanov, I.V., Clayton, R.H., Nash, M.P., Bradley, C.P., Paterson, D.J., Hayward, M.P., Taggart, P., Panfilov, A.V., 2014. Effect of global cardiac ischemia on human ventricular fibrillation: insights from a multi-scale mechanistic model of the human heart. PLoS Comput. Biol. 10.
Kimura, S., Bassett, A.L., Furukawa, T., Cuevas, J., Myerburg, R.J., 1990. Electrophysiological properties and responses to simulated ischemia in cat ventricular myocytes of endocardial and epicardial origin. Circ. Res. 66, 469–477. http://dx.doi.org/10.1161/01.res.66.2.469.
Kleber, A.G., 1983. Resting membrane potential, extracellular potassium activity, and intracellular sodium activity during acute global ischemia in isolated perfused guinea pig hearts. Circ. Res. 52, 442–450.
Kodama, I., Wilde, A., Janse, M., Durrer, D., Yamada, K., 1984. Combined effects of hypoxia, hyperkalemia and acidosis on membrane action potential and excitability of guinea-pig ventricular muscle. J. Mol. Cell. Cardiol. 16, 247–259. http://dx.doi.org/10.1016/s0022-2828(84)80591-x.
Kurz, R.W., Mohabir, R., Ren, X.L., Franz, M.R., 1993. Ischaemia induced alternans of action potential duration in the intact-heart: dependence on coronary flow, preload and cycle length. Eur. Heart J. 14, 1410–1420.
Kurz, R.W., Ren, X.L., Franz, M.R., 1994. Dispersion and delay of electrical restitution in the globally ischaemic heart. Eur. Heart J. 15, 547–554.
Lab, M.J., Woollard, K.V., 1978. Monophasic action potentials, electrocardiograms and mechanical performance in normal and ischaemic epicardial segments of the pig ventricle in situ. Cardiovasc. Res. 12, 555–565. http://dx.doi.org/10.1093/cvr/12.9.555.
Ma, L., Wang, L., 2007. Effect of acute subendocardial ischemia on ventricular refractory periods. Exp. Clin. Cardiol. 12, 63–66.
Michailova, A., Lorentz, W., McCulloch, A., 2007. Modeling transmural heterogeneity of KATP current in rabbit ventricular myocytes. Am. J. Physiol. Cell Physiol. 293, C542–557. http://dx.doi.org/10.1152/ajpcell.00148.2006.
Moréna, H., Janse, M.J., Fiolet, J.W., Krieger, W.J., Crijns, H., Durrer, D., 1980. Comparison of the effects of regional ischemia, hypoxia, hyperkalemia, and acidosis on intracellular and extracellular potentials and metabolism in the isolated porcine heart. Circ. Res. 46, 634–646.
Nademanee, K., Feld, G., Hendrickson, J., Singh, P.N., Singh, B.N., 1985. Electrophysiologic and antiarrhythmic effects of sotalol in patients with life-threatening ventricular tachyarrhythmias. Circulation 72, 555–564. http://dx.doi.org/10.1161/01.cir.72.3.555.
Nakashima, M., Hashimoto, H., Kanamaru, M., Nagaya, T., Hashizume, M., Oishi, H., 1978. Experimental studies and clinical report on the electrical alternans of ST segment during myocardial ischemia. Jpn. Heart J. 19, 396–408.
Niederer, S.A., Fink, M., Noble, D., Smith, N.P., 2009. A meta-analysis of cardiac electrophysiology computational models. Exp. Physiol. 94, 486–495. http://dx.doi.org/10.1113/expphysiol.2008.044610.
O'Hara, T., Rudy, Y., 2012. Quantitative comparison of cardiac ventricular myocyte electrophysiology and response to drugs in human and nonhuman species. Am. J. Physiol. - Heart Circ. Physiol. 302, H1023–H1030. http://dx.doi.org/10.1152/ajpheart.00785.2011.
O'Hara, T., Virág, L., Varró, A., Rudy, Y., 2011. Simulation of the undiseased human cardiac ventricular action potential: model formulation and experimental validation. PLoS Comput. Biol. 7, e1002061+. http://dx.doi.org/10.1371/journal.pcbi.1002061.
Pandit, S.V., Kaur, K., Zlochiver, S., Noujaim, S.F., Furspan, P., Mironov, S., Shibayama, J., Anumonwo, J., Jalife, J., 2011. Left-to-right ventricular differences in IKATP underlie epicardial repolarization gradient during global ischemia. Heart Rhythm 8, 1732–1739. http://dx.doi.org/10.1016/j.hrthm.2011.06.028.
Pandit, S.V., Warren, M., Mironov, S., Tolkacheva, E.G., Kalifa, J., Berenfeld, O., Jalife, J., 2010. Mechanisms underlying the antifibrillatory action of hyperkalemia in Guinea pig hearts. Biophys. J. 98, 2091–2101. http://dx.doi.org/10.1016/j.bpj.2010.02.011.
Passini, E., Mincholé, A., Coppini, R., Cerbai, E., Rodriguez, B., Severi, S., Bueno-Orovio, A., 2016. Mechanisms of pro-arrhythmic abnormalities in ventricular repolarisation and anti-arrhythmic therapies in human hypertrophic cardiomyopathy. J. Mol. Cell. Cardiol. 96, 72–81. http://dx.doi.org/10.1016/j.yjmcc.2015.09.003.
Pathmanathan, P., Bernabeu, M.O., Bordas, R., Cooper, J., Garny, A., Pitt-Francis, J.M., Whiteley, J.P., Gavaghan, D.J., 2010. A numerical guide to the solution of the bi-domain equations of cardiac electrophysiology. Prog. Biophys. Mol. Biol. 102, 136–155. http://dx.doi.org/10.1016/j.pbiomolbio.2010.05.006.
Penny, W.J., Sheridan, D.J., 1983. Arrhythmias and cellular electrophysiological changes during myocardial "ischaemia" and reperfusion. Cardiovasc. Res. 17, 363–372. http://dx.doi.org/10.1093/cvr/17.6.363.
Pitt-Francis, J., Pathmanathan, P., Bernabeu, M.O., Bordas, R., Cooper, J., Fletcher, A.G., Mirams, G.R., Murray, P., Osborne, J.M., Walter, A., Chapman, S.J., Garny, A., van Leeuwen, I.M.M., Maini, P.K., Rodríguez, B., Waters, S.L., Whiteley, J.P., Byrne, H.M., Gavaghan, D.J., 2009. Chaste: a test-driven approach to software development for biological modelling. Comput. Phys. Commun. 180, 2452–2471. http://dx.doi.org/10.1016/j.cpc.2009.07.019.
Pogwizd, S.M., Corr, P.B., 1987. Reentrant and nonreentrant mechanisms contribute to arrhythmogenesis during early myocardial ischemia: results using three-dimensional mapping. Circ. Res. 61, 352–371.
Quinn, T.A., Kohl, P., 2013. Combining wet and dry research: experience with model development for cardiac mechano-electric structure-function studies. Cardiovasc. Res. 97, 601–611. http://dx.doi.org/10.1093/cvr/cvt003.
Rodriguez, B., Carusi, A., Abi-Gerges, N., Ariga, R., Britton, O., Bub, G., Bueno-Orovio, A., Burton, R.A.B., Carapella, V., Cardone-Noott, L., Daniels, M.J.,

Davies, M.R., Dutta, S., Ghetti, A., Grau, V., Harmer, S., Kopljar, I., Lambiase, P., Lu, H.R., Lyon, A., Minchole, A., Muszkiewicz, A., Oster, J., Paci, M., Passini, E., Severi, S., Taggart, P., Tinker, A., Valentin, J.-P., Varro, A., Wallman, M., Zhou, X., 2016. Human-based Approaches to Pharmacology and Cardiology: an Interdisciplinary and Intersectorial Workshop. Europace 18 (9), 1287–1298. http://dx.doi.org/10.1093/europace/euv320.

Sato, R., Noma, A., Kurachi, Y., Irisawa, H., 1985. Effects of intracellular acidification on membrane currents in ventricular cells of the Guinea pig. Circ. Res. 57, 553–561.

Schaapherder, A.F.M., Schumacher, C.A., Coronel, R., Fiolet, J.W.T., 1990. Transmural inhomogeneity of extracellular [K+] and pH and myocardial energy metabolism in the isolated rat heart during acute global ischemia; dependence on gaseous environment. Basic Res. Cardiol. 85, 33–44. http://dx.doi.org/10.1007/bf01907012.

Shannon, T.R., Wang, F., Puglisi, J., Weber, C., Bers, D.M., 2004. A mathematical treatment of integrated Ca dynamics within the ventricular myocyte. Biophys. J. 87, 3351–3371. http://dx.doi.org/10.1529/biophysj.104.047449.

Shaw, R.M., Rudy, Y., 1997. Electrophysiologic effects of acute myocardial ischemia. A mechanistic investigation of action potential conduction and conduction failure. Circ. Res. 80, 124–138.

Sutton, P.M., Taggart, P., Opthof, T., Coronel, R., Trimlett, R., Pugsley, W., Kallis, P., 2000. Repolarisation and refractoriness during early ischaemia in humans. Heart Br. Card. Soc. 84, 365–369.

Taggart, P., 2000. Inhomogeneous transmural conduction during early ischaemia in patients with coronary artery disease. J. Mol. Cell. Cardiol. 32, 621–630. http://dx.doi.org/10.1006/jmcc.2000.1105.

Taggart, P., Slater, J.D., 1971. Significance of potassium in genesis of arrhythmias in induced cardiac ischaemia. Br. Med. J. 4, 195–198.

ten Tusscher, K.H., Noble, D., Noble, P.J., Panfilov, A.V., 2004. A model for human ventricular tissue. Am. J. Physiol. Heart Circ. Physiol. 286, H1573–H1589. http://dx.doi.org/10.1152/ajpheart.00794.2003.

ten Tusscher, K., Bernus, O., Hren, R., Panfilov, A., 2006. Comparison of electrophysiological models for human ventricular cells and tissues. Prog. Biophys. Mol. Biol. 90, 326–345. http://dx.doi.org/10.1016/j.pbiomolbio.2005.05.015.

Terkildsen, J.R., Niederer, S., Crampin, E.J., Hunter, P., Smith, N.P., 2008. Using Physiome standards to couple cellular functions for rat cardiac excitation–contraction. Exp. Physiol. 93, 919–929. http://dx.doi.org/10.1113/expphysiol.2007.041871.

Tice, B.M., Rodríguez, B., Eason, J., Trayanova, N., 2007. Mechanistic investigation into the arrhythmogenic role of transmural heterogeneities in regional ischaemia phase 1A. Europace 9, vi46–vi58. http://dx.doi.org/10.1093/europace/eum204.

Tran, K., Smith, N.P., Loiselle, D.S., Crampin, E.J., 2009. A thermodynamic model of the cardiac sarcoplasmic/endoplasmic Ca2+ (SERCA) pump. Biophys. J. 96, 2029–2042. http://dx.doi.org/10.1016/j.bpj.2008.11.045.

Trénor, B., Ferrero, J.M., Rodríguez, B., Montilla, F., 2005. Effects of pinacidil on reentrant arrhythmias generated during acute regional ischemia: a simulation study. Ann. Biomed. Eng. 33, 897–906.

ten Tusscher, K.H.W.J., Panfilov, A.V., 2006. Alternans and spiral breakup in a human ventricular tissue model. Am. J. Physiol. - Heart Circ. Physiol. 291, H1088–H1100. http://dx.doi.org/10.1152/ajpheart.00109.2006.

Van Wagoner, D.R., Lamorgese, M., 1994. Ischemia potentiates the mechanosensitive modulation of atrial atp-sensitive potassium channels a. Ann. N. Y. Acad. Sci. 723, 392–395. http://dx.doi.org/10.1111/j.1749-6632.1994.tb36755.x.

Vermeulen, J., 1996. Electrophysiologic and extracellular ionic changes during acute ischemia in failing and normal rabbit myocardium. J. Mol. Cell. Cardiol. 28, 123–131. http://dx.doi.org/10.1006/jmcc.1996.0012.

Wagner, S., Dybkova, N., Rasenack, E.C., Jacobshagen, C., Fabritz, L., Kirchhof, P., Maier, S.K., Zhang, T., Hasenfuss, G., Brown, J.H.H., Bers, D.M., Maier, L.S., 2006. Ca^{2+}/calmodulin-dependent protein kinase II regulates cardiac Na+ channels. J. Clin. Invest 116, 3127–3138. http://dx.doi.org/10.1172/jci26620.

Watanabe, I., Kanda, A., Engle, C.L., Gettes, L.S., 1997. Comparison of the effects of regional ischemia and hyperkalemia on the membrane action potentials of the in situ pig heart. J. Cardiovasc. Electrophysiol. 8, 1229–1236. http://dx.doi.org/10.1111/j.1540-8167.1997.tb01012.x.

Weiss, J., Shine, K.I., 1982. [K+]o accumulation and electrophysiological alterations during early myocardial ischemia. Am. J. Physiol. Heart Circ. Physiol. 243, H318–H327.

Weiss, J.N., Venkatesh, N., Lamp, S.T., 1992. ATP-sensitive K+ channels and cellular K+ loss in hypoxic and ischaemic mammalian ventricle. J. Physiol. 447, 649–673.

Wilde, A.A., Escande, D., Schumacher, C.A., Thuringer, D., Mestre, M., Fiolet, J.W., Janse, M.J., 1990. Potassium accumulation in the globally ischemic mammalian heart. A role for the ATP-sensitive potassium channel. Circ. Res. 67, 835–843.

Wilensky, R.L., Tranum-Jensen, J., Coronel, R., Wilde, A.A., Fiolet, J.W., Janse, M.J., 1986. The subendocardial border zone during acute ischemia of the rabbit heart: an electrophysiologic, metabolic, and morphologic correlative study. Circulation 74, 1137–1146.

Xie, Y., Sato, D., Garfinkel, A., Qu, Z., Weiss, J.N., 2010. So little source, so much sink: requirements for afterdepolarizations to propagate in tissue. Biophys. J. 99, 1408–1415. http://dx.doi.org/10.1016/j.bpj.2010.06.042.

Yatani, A., Brown, A.M., Akaike, N., 1984. Effect of extracellular pH on sodium current in isolated, single rat ventricular cells. J. Membr. Biol. 78, 163–168. http://dx.doi.org/10.1007/bf01869203.

Zaitsev, A.V., Guha, P.K., Sarmast, F., Kolli, A., Berenfeld, O., Pertsov, A.M., de Groot, J.R., Coronel, R., Jalife, J., 2003. Wavebreak formation during ventricular fibrillation in the isolated, regionally ischemic pig heart. Circ. Res. 92, 546–553. http://dx.doi.org/10.1161/01.res.0000061917.23107.f7.

Zhou, X., Bueno-Orovio, A., Orini, M., Hanson, B., Hayward, M., Taggart, P., Lambiase, P.D., Burrage, K., Rodriguez, B., 2016. In vivo and in silico investigation into mechanisms of frequency dependence of repolarization alternans in human ventricular cardiomyocytes novelty and significance. Circ. Res. 118, 266–278. http://dx.doi.org/10.1161/circresaha.115.307836.